

ReBA-Pred-Net: Weakly-Supervised Regional Brain Age Prediction on MRI

Shuai Shao¹ Yan Wang² Shu Jiang³ Shiyuan Zhao⁴ Xinzhe Luo¹ Di Yang¹
 Jiangtao Wang¹ Yutong Bai⁵ Jianguo Zhang⁵

Abstract

Brain age has become a prominent biomarker of brain health. Yet most prior work targets whole brain age (WBA), a coarse paradigm that struggles to support tasks such as disease characterization and research on development and aging patterns, because relevant changes are typically region-selective rather than brain-wide. Therefore, robust regional brain age (ReBA) estimation is critical, yet a widely generalizable model has yet to be established. In this paper, we propose the **Regional Brain Age Prediction Network (ReBA-Pred-Net)**, a Teacher-Student framework designed for fine-grained brain age estimation. The Teacher produces soft ReBA to guide the Student to yield reliable ReBA estimates with a clinical-prior consistency constraint (regions within the same function should change similarly). For rigorous evaluation, we introduce two indirect metrics: **Healthy Control Similarity (HCS)**, which assesses statistical consistency by testing whether regional brain-age-gap (ReBA minus chronological age) distributions align between training and unseen HC; and **Neuro Disease Correlation (NDC)**, which assesses factual consistency by checking whether clinically confirmed patients show elevated brain-age-gap in disease-associated regions. Experiments across multiple backbones demonstrate the statistical and factual validity of our method.

1. Introduction

As individuals age, the human brain undergoes progressive senescence, such as reductions in gray-matter volume, de-

^{*}Equal contribution ¹University of Science and Technology of China, Hefei, China ²Beijing Jiaotong University, Beijing, China

³China University of Petroleum (East China), Qingdao, China

⁴Northwestern Polytechnical University, Xian, China ⁵Beijing Tiantan Hospital, Beijing, China. Correspondence to: Yan Wang <wangyan9509@gmail.com>, Jiangtao Wang <wangjiangtao@ustc.edu.cn>, Jianguo Zhang <zjguo73@126.com>.

Preliminary work.

generation of white-matter microstructure, and remodeling of functional connectivity. To quantitatively characterize these age-related alterations, researchers have introduced the *Brain Age* representation that maps neuroimaging features (e.g., Magnetic Resonance Imaging, MRI) to chronological age in healthy control (HC) (Wang et al., 2025; Lee et al., 2022a; Bethlehem et al., 2022). The difference between brain age and chronological age (Brain Age Gap) indicates whether a brain appears “older” or “younger” than expected and has become an important composite biomarker for assessing brain health.

Conventional brain age prediction typically treats the whole-brain as the analytical unit, yet such a coarse-grained paradigm struggles to support many neuroscientific tasks: (i) Brain aging patterns. Brain maturation and senescence are heterogeneous. Brain regions differ in maturation timelines, peak volumes, and atrophy rates (e.g., sensorimotor-related brain regions often peak earlier than prefrontal brain regions). Whole Brain Age (WBA) cannot reveal these asynchronous, region-specific timelines and rate differences. (ii) Disease-level analysis. Pathological changes in neurological disorders are region-selective rather than brain-wide. e.g., Parkinson’s disease (PD) primarily involves motor-related regions, whereas Alzheimer’s disease (AD) is closely linked to memory-related structures. However, WBA cannot localize affected regions, making it difficult to support pathological interpretation and clinical decision-making. Therefore, *moving to a finer spatial granularity with Regional Brain Age (ReBA) prediction*, is vital for both neuroscience research and clinical applications (see Fig. 1 (a)).

Recently, WBA prediction is relatively mature, whereas ReBA estimation remains nascent. Existing approaches are either purely conceptual (Bethlehem et al., 2022; Kalc et al., 2024) or rely on pre-extracted morphological features (e.g., volume, thickness) (Riccardi et al., 2025; Lee et al., 2022b), which suffer from spatial information loss and poor generalizability due to scanner and pipeline sensitivities. We aim to design a feature-engineering-free deep-learning-based framework operating directly on raw 3D MRI.

However, realizing this goal exposes a *fundamental bottleneck: the absence of observable ground-truth labels for ReBA*. This limitation means our only viable option is to use

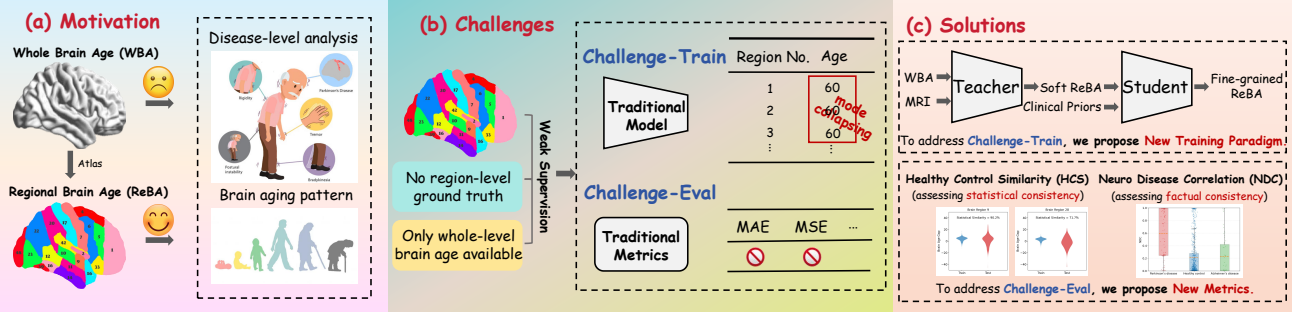


Figure 1. (a) Motivation. The coarse WBA cannot adequately support disease-level analyses or studies of aging. Parcellating the brain with established functional atlases and modeling ReBA has the potential to solve these limitations and to strengthen brain-health research. **(b) Challenges.** ReBA lacks region-level ground truth. In training, HC chronological age is the only available weak signal, risking mode collapsing and obscuring true regional differences; in evaluation, the absence of regional truth prevents region-wise supervision, making standard metrics (e.g., MAE/MSE) inapplicable. **(c) Solutions.** We propose ReBA-Pred-Net with Teacher-Student framework to address the training problem, and introduce two evaluation metrics, HCS and NDC, to assess statistical consistency and factual consistency.

HC' chronological age as weak supervision to predict ReBA, which unavoidably brings substantial challenges for training and evaluation (see Fig. 1 (b)). **Challenge-Train:** When all regions share the same brain age label, the model collapses to an over-averaged solution, obscuring regional differences and spatial gradients and thus degrading predictive performance. **Challenge-Eval:** Without region-level ground truth, region-wise supervised evaluation is impossible, and standard metrics, such as mean absolute error (MAE), are inapplicable for assessing ReBA estimates.

To address Challenge-Train, we propose the Regional Brain Age Prediction Network (**ReBA-Pred-Net**, see Fig. 1 (c)), which estimates ReBA under whole-brain level weak supervision using a Teacher-Student framework.

(i) The Teacher module (see Fig. 2 Top) converts weakly-supervised WBA into region-wise soft targets (*directly optimizing based on the WBA invites shortcut learning and degenerate solutions*). After standard preprocessing (skull stripping, N4 bias correction, and nonlinear registration by DeepPrep (Ren et al., 2025)), we train the Teacher to regress WBA using HC's chronological age and then freeze its weights. We then parcellate the brain with the atlas (e.g., Harvard-Oxford (Jenkinson et al., 2012)) and use the frozen Teacher on each region to obtain initial ReBA. Next, we apply an additive correction to each region according to its marginal contribution to the whole-brain prediction (*i.e.*, the perturb-and-observe change in WBA after lightly occluding that region), yielding more reliable soft ReBA. This procedure mitigates over-averaging and turns global weak supervision into localized, teachable signals.

(ii) The Student module (see Fig. 2 Bottom) implements fine-grained regional estimation. On a shared backbone, we introduce a learnable prompt to each brain region, use it to perform Feature-wise Linear Modulation (FiLM), and employ a lightweight adapter to produce region-specific readouts.

The Student is trained to match the Teacher's corrected soft ReBA via a distillation loss. In addition, we impose a functional consistency constraint, encouraging regions within the same functional system (e.g., vision-related regions) to have similar ages, which suppresses over-averaging and preserves plausible spatial gradients.

For Challenge-Eval, we present two complementary indirect metrics (see Fig. 1 (c)): **Healthy Control Similarity (HCS)**, assessing statistical consistency; and **Neuro Disease Correlation (NDC)**, assessing factual consistency.

(i) HCS is evaluated on unseen HC. We compute the Regional Brain Age Gap (Δ ReBA, ReBA minus chronological age) and compare its distribution against the HC training data. If the two distributions align, the model is well-calibrated on HC with no evident distributional drift. *Note that, although this metric has limitations at the individual level, it captures group-level statistical consistency and thus serves as an effective gatekeeper for basic model reliability.*

(ii) NDC is evaluated on clinically confirmed neuro disorders. Using clinical priors to specify the disease-related region set (e.g., motor-related regions for PD, memory-related regions for AD, see Sec. D), we compute the Δ ReBA individually within this set. When this gap is larger and significantly exceeds that of HC and non-target disease groups, the model's ReBA pattern accords with the known disease prior, providing evidence for validity. *Intuitively, in the absence of regional ground truth, we substitute “known facts” for “unknown labels”: NDC tests whether regions that should appear “older” indeed do so; satisfying this criterion supports the credibility of the model’s predictions.*

Our main contributions are summarized as follows:

- We identify the central obstacle in ReBA research as the lack of fine-grained region-level labels, and we cast this into two methodological challenges, *i.e.*, Challenge-Train and Challenge-Eval.

- We present ReBA-Pred-Net for Challenge-Train, a Teacher-Student framework in which the Teacher, trained under whole-brain weak supervision, produces soft ReBA, and the Student employs region-specific prompts with consistency constraints, enabling reliable ReBA estimation despite weak supervision.
- We design HCS and NDC for Challenge-Eval. HCS emphasizes statistical consistency, whereas NDC emphasizes factual consistency; together they provide complementary, testable validation when region-level ground truth is unavailable. Empirical results demonstrate the effectiveness of our method.

2. Related Work

Whole brain age (WBA). Research on WBA is relatively mature. Early work used voxel-based morphometry (VBM) features (Ashburner & Friston, 2000; Good et al., 2001; Pennanen et al., 2005), for example counts or summaries of gray and white matter at the voxel level, to regress age. These pipelines were limited by hand-crafted descriptors, sensitivity to smoothing and partial-volume effects, and site or scanner variability, which constrained accuracy. Subsequent studies adopted classical machine-learning regressors such as Gaussian processes (Cole et al., 2015), hidden Markov models (Wang & Pham, 2011), and random forests (Liem et al., 2017), typically trained on VBM or global features extracted from T1-weighted MRI. With larger cohorts and greater compute, deep learning became the standard approach, where 3D CNNs and Transformer-based architectures take MRI as input and directly regress WBA (Lee et al., 2022a; Cheng et al., 2021; Armanious et al., 2021; Jónsson et al., 2019; Kuchcinski et al., 2023; Yu et al., 2024; Seitz-Holland et al., 2024). Evaluation protocols are well established, commonly reporting MAE, MSE, and Spearman’s rank correlation coefficient (SRCC) etc.

Regional brain age (ReBA). *In contrast to the mature field of WBA prediction, ReBA estimation remains at a nascent stage.* Existing efforts to characterize regional aging fall predominantly into two categories: purely conceptual discussions (Bethlehem et al., 2022; Kalc et al., 2024) and morphological feature-based methods (Riccardi et al., 2025; Lee et al., 2022b). For the former, Bethlehem *et al.* map normative trajectories of region-level morphometry across the human lifespan, and Kalc *et al.* outline best practices for brain-age workflows. However, these studies focus on macro-level cohort statistics rather than providing an actionable predictive model for individual-level ReBA estimation. For the latter, existing computational approaches rely on a two-stage paradigm using pre-extracted morphological features (*e.g.*, cortical thickness and volume derived from FreeSurfer (Fischl, 2012)). This approach inherently suffers from significant spatial information loss (discarding texture and intensity gradients) and cumulative errors originating

from segmentation and registration steps. Consequently, these models exhibit poor cross-site generalizability due to their high sensitivity to scanner variations and preprocessing pipelines. These limitation underscores the urgent need for a general-purpose ReBA framework with standardized validation; our study addresses this by proposing ReBA-Pred-Net and introducing complementary metrics (HCS and NDC).

3. Methodology

3.1. Overview

We propose the Regional Brain Age Prediction Network (**ReBA-Pred-Net**), which comprises three components:

- (i) Preprocessing module (Please see Sec. C) applies Deep-Prep (Ren et al., 2025) for skull stripping, N4 bias correction and nonlinear registration on T1-weighted MRI to standardize anatomy (Avants et al., 2009).
- (ii) Teacher module (Please see Fig. 2 Top) trains a WBA regressor with chronological age, freezes it, derives per-region initial ReBA with atlas parcellation, and then applies additive corrections to obtain soft ReBA.
- (iii) Student module (Please see Fig. 2 Bottom) shares the backbone with the Teacher, extracts regional embeddings, injects learnable prompts and feature-wise linear modulation, fuses features, and uses a lightweight adapter to output fine-grained ReBA; it is optimized with distillation to soft ReBA plus a functional-consistency loss (regions in the same functional network should change similarly).

3.2. MRI Pre-processing Module

MRI scans vary in resolution, contrast, and signal-to-noise ratio across scanners, and also differ in anatomy between subjects. We therefore standardize all raw T1-weighted images with MRI-Processor to improve robustness and cross-subject comparability. Define the raw MRI image as $\mathbf{X}_{\text{raw}} \in \mathbb{R}^{D \times H \times W}$, the workflow is:

$$\mathbf{X}_{\text{proc}} = \mathcal{F}_{\text{DeepPrep}}(\mathbf{X}_{\text{raw}}), \quad (1)$$

where $\mathbf{X}_{\text{proc}} \in \mathbb{R}^{D \times H \times W}$ denotes the processed MRI data, D, H, W represent the depth, height, and width; $\mathcal{F}_{\text{DeepPrep}}$ denotes the operation of using DeepPrep to implement brain extraction, bias field correction, and nonlinear registration.

3.3. Teacher Module

Workflow. Define the teacher module as \mathbb{T} . Its purpose is to produce soft ReBA for fine-grained supervision of the Student via a five-step pipeline. By converting coarse whole-brain supervision into regional signals, it avoids collapsing all regions to a single chronological-age label and enhances region-specific discrimination. *The key challenge is obtaining reliable soft labels, otherwise it is “garbage in, garbage*

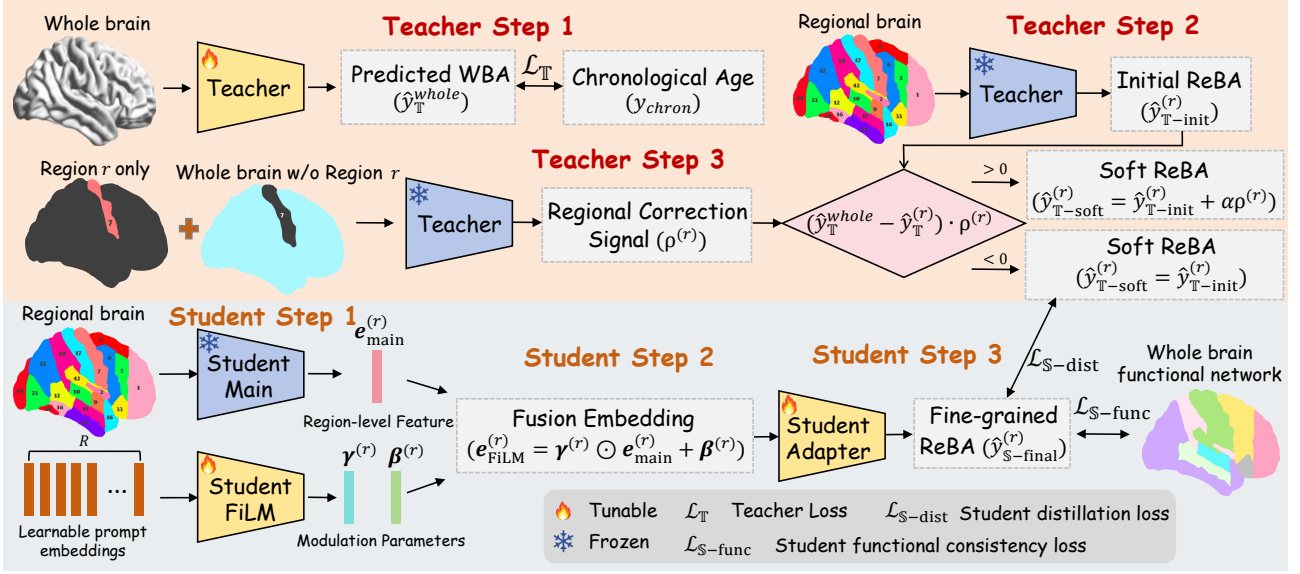


Figure 2. The flowchart of Regional Brain Age Prediction Network (ReBA-Pred-Net). **Teacher module** consists of three decoupled steps: (i) Feed the whole-brain MRI to the Teacher to predict WBA and train it against chronological age; (ii) Parcellate the brain using an atlas; extract each region and pass it through the frozen Teacher to obtain initial ReBA; (iii) Apply the corrections in Eqs. (7), (8) to each region to produce the final soft ReBA. **Student module** comprises three sequential steps: (i) Feed each region to the Student Main (shared with the Teacher) to obtain a regional embedding; (ii) Add a learnable prompt per region, generate modulated parameters with a tunable Student FiLM, and fuse them with the regional embedding; (iii) Pass the fused feature through a lightweight adapter to produce the final fine-grained ReBA. We optimize the Student with a distillation loss (to match the Teacher’s soft ReBA) and a functional-consistency loss (enforcing that regions within the same functional network change similarly). **Notably, all training is conducted exclusively on HC.**

out”. We first derive initial ReBA (Step iii), then refine it with an additive correction signal (Step iv), yielding the final soft ReBA used for supervision (Step v). **Notably, all training is conducted exclusively on HC.**

(i) We begin by training the Teacher (model-agnostic) on the processed training data \mathbf{X}_{proc} to predict WBA. It is trained by minimizing the discrepancy between this prediction and the chronological age. Upon convergence, the model’s parameters are frozen for subsequent stages. The estimated WBA can be formulated as:

$$\hat{y}_T^{(whole)} = \mathbf{T}(\mathbf{X}_{\text{proc}}), \quad (2)$$

where $\hat{y}_T^{(whole)}$ denotes the estimated whole-brain age.

(ii) Define the atlas as $\mathbf{M}_{\text{raw}} \in \mathbb{R}^{D \times H \times W}$, where each voxel is assigned an integer label from 0 to R , corresponding to one of R brain regions, *i.e.*, $\mathbf{M}_{\text{raw}}[i, j, k] \in \{0, 1, 2, \dots, R\}$. We perform one-hot encoding for the atlas, which can be formulated as:

$$\mathbf{M}_{\text{proc}} = \mathcal{F}_{\text{onehot}}(\mathbf{M}_{\text{raw}}), \quad (3)$$

where $\mathbf{M}_{\text{proc}} \in \mathbb{R}^{R \times D \times H \times W}$ denotes the one-hot atlas.

(iii) Subsequently, the one-hot atlas is used to isolate voxel sets for each brain region. To reduce boundary artifacts, the brain region mask is dilated by 1 voxel, and all non-selected

regions are replaced with small noise (η). The process can be formulated as:

$$\mathbf{X}_{\text{proc}}^{(r)} = \mathbf{X}_{\text{proc}} \odot \mathbf{M}_{\text{proc}}^{(r)} + \eta \mathbf{Z} \odot (1 - \mathbf{M}_{\text{proc}}^{(r)}), \quad (4)$$

where $\mathbf{X}_{\text{proc}}^{(r)}$, $\mathbf{M}_{\text{proc}}^{(r)}$ denote the processed brain image and the atlas mask of the r -th region, respectively; $\mathbf{Z} \sim \mathcal{N}(0, 1)$, and $\eta \ll 1$. Following, we use the Teacher to predict the initial ReBA of the r -th brain region by:

$$\hat{y}_{T-init}^{(r)} = \mathbf{T}(\mathbf{X}_{\text{proc}}^{(r)}). \quad (5)$$

(iv) Meanwhile, we introduce a regional correction signal to quantify each brain region’s influence on WBA estimation. *Intuitively, if the r -th region is “occluded” (e.g., replaced with small noise so that the teacher cannot perceive it), we measure how much the teacher’s WBA prediction changes. A positive value indicates that the region’s age should be higher than the WBA estimate; a negative value indicates it should be lower. This change serves as an auxiliary correction signal for ReBA prediction.* Formally, let the occluded input be:

$$\mathbf{X}_{\text{proc}}^{(-r)} = \mathbf{X}_{\text{proc}} \odot (1 - \mathbf{M}_{\text{proc}}^{(r)}) + \eta \mathbf{Z} \odot \mathbf{M}_{\text{proc}}^{(r)}. \quad (6)$$

This regional correction signal can be formulated as:

$$\rho^{(r)} = \mathbb{E}_{(\mathbf{X}_{\text{proc}} \sim \mathcal{D}_{\text{tr}})} [\mathbf{T}(\mathbf{X}_{\text{proc}}) - \mathbf{T}(\mathbf{X}_{\text{proc}}^{(-r)})], \quad (7)$$

where $\rho^{(r)} > 0$ means the r -th brain region increases the predicted age, whereas $\rho^{(r)} < 0$ lowers the prediction; \mathcal{D}_{tr} denotes the training data; $\mathbb{E}_{(\cdot)}$ is the expectation operator; $\mathbb{E}_{(\mathbf{X}_{\text{proc}} \sim \mathcal{D}_{\text{tr}})} [\cdot]$ indicates that, for every training example, we compute the correction signal for region r and subsequently take the average across the dataset.

(v) Finally, we correct the ReBA using this regional correction signal, which can be formulated as:

$$\hat{y}_{\mathbf{T}-\text{soft}}^{(r)} = \hat{y}_{\mathbf{T}-\text{init}}^{(r)} + \mathbb{1}_{((\hat{y}_{\mathbf{T}}^{(\text{whole})} - \hat{y}_{\mathbf{T}-\text{init}}^{(r)}) \cdot \rho^{(r)} > 0)} \cdot \alpha \rho^{(r)}, \quad (8)$$

where $\mathbb{1}_{(\text{condition})}$ is the indicator function, equal to 1 if the condition is true and 0 otherwise; α is the hyperparameter. Put simply, the $\mathbb{1}_{((\hat{y}_{\mathbf{T}}^{(\text{whole})} - \hat{y}_{\mathbf{T}-\text{init}}^{(r)}) \cdot \rho^{(r)} > 0)}$ is used to check whether the direction of the predicted ReBA is consistent with the correction signal; if consistent, no update is applied, and otherwise, the prediction is adjusted toward the signal with a step size of $\alpha \rho^{(r)}$.

Teacher Loss. During the teacher stage, we only minimize the MAE loss between the chronological age and the WBA predicted by the model, which can be formulated as:

$$\mathcal{L}_{\mathbf{T}} = \frac{1}{N} \sum_{n=1}^N \left| \hat{y}_{\mathbf{T}}^{(\text{whole}, n)} - y_{\text{chron}}^{(n)} \right|, \quad (9)$$

where $\hat{y}_{\mathbf{T}}^{(\text{whole}, n)}$, $y_{\text{chron}}^{(n)}$ denote the predicted WBA and chronological age of the n -th subject. After training, the teacher's parameters are fully frozen. In the Eqs. (5) and (7), we directly invoke this frozen teacher to obtain the ReBA.

3.4. Student Module

Workflow. Define the student module as \mathbf{S} , which performs on-demand ReBA prediction. It consists of three components: a teacher-inspired main block, a Feature-wise Linear Modulation (FiLM) block, and an adapter block, which can be formulated as:

$$\mathbf{S} = \{\mathbf{S}_{\text{main}}, \mathbf{S}_{\text{FiLM}}, \mathbf{S}_{\text{adapter}}\}. \quad (10)$$

\mathbf{S}_{main} shares the same backbone parameters as the teacher \mathbf{T} but removes the regression head and remains frozen; \mathbf{S}_{FiLM} and $\mathbf{S}_{\text{adapter}}$ are trainable. The workflow has three steps:

(i) First, following Eq. (4), we extract the voxels corresponding to each brain region. The resulting single region is then fed into the student main block to obtain a regional feature embedding. This yields a compact and stable region-level feature vector used for subsequent adapter-based prediction. We formulate the process as:

$$\mathbf{e}_{\text{main}}^{(r)} = \mathbf{S}_{\text{main}} \left(\mathbf{X}_{\text{proc}}^{(r)} \right), \quad (11)$$

where $\mathbf{e}_{\text{main}}^{(r)} \in \mathbb{R}^{d_m}$ is the r -th brain region embedding.

(ii) Subsequently, for each brain region, we introduce a learnable prompt embedding ($\mathbf{p}^{(r)} \in \mathbb{R}^{d_p}$) and feed it into a lightweight FiLM block to produce the modulated parameters. These parameters are then used to apply feature-wise affine modulation to the previously extracted regional feature embeddings. *Intuitively, the block learns how to generate region-specific readout rules from the regional prompt, thereby scaling and shifting each region's features while sharing a single regression head. This design preserves region specificity, enables parameter sharing for efficiency, and fits naturally with a prompt-as-inference interface, yielding more stable and interpretable ReBA estimates.* The process can be formulated as:

$$\gamma^{(r)}, \beta^{(r)} = \mathbf{S}_{\text{FiLM}} \left(\mathbf{p}^{(r)} \right), \quad (12)$$

$$\mathbf{e}_{\text{FiLM}}^{(r)} = \gamma^{(r)} \odot \mathbf{e}_{\text{main}}^{(r)} + \beta^{(r)}, \quad (13)$$

where $\gamma^{(r)}, \beta^{(r)} \in \mathbb{R}^{d_m}$ are the modulation parameters; $\mathbf{e}_{\text{FiLM}}^{(r)} \in \mathbb{R}^{d_m}$ indicates the fusion embedding; \mathbf{S}_{FiLM} is implemented as a multilayer perceptron (MLP).

(iii) Finally, based on the fused regional features, we build a single lightweight adapter shared across all brain regions to output the final ReBA:

$$\hat{y}_{\mathbf{S}-\text{final}}^{(r)} = \mathbf{S}_{\text{adapter}} \left(\mathbf{e}_{\text{FiLM}}^{(r)} \right), \quad (14)$$

where $\mathbf{S}_{\text{adapter}}$ is realized as a MLP.

Student Loss The student loss comprises two components, which can be formulated as:

$$\mathcal{L}_{\mathbf{S}} = \mathcal{L}_{\mathbf{S}-\text{dist}} + \zeta \mathcal{L}_{\mathbf{S}-\text{func}}, \quad (15)$$

where ζ is the hyperparameter.

(i) $\mathcal{L}_{\mathbf{S}-\text{dist}}$ indicates the distillation loss, encouraging the student's ReBA predictions to fit the teacher's soft ReBA, which can be formulated as:

$$\mathcal{L}_{\mathbf{S}-\text{dist}} = \frac{1}{R \times N} \sum_{r=1}^R \sum_{n=1}^N \left| \hat{y}_{\mathbf{S}-\text{final}}^{(r, n)} - \hat{y}_{\mathbf{T}-\text{soft}}^{(r, n)} \right|, \quad (16)$$

where $\hat{y}_{\mathbf{S}-\text{final}}^{(r, n)}$, $\hat{y}_{\mathbf{T}-\text{soft}}^{(r, n)}$ denote the predicted ages for subject n and region r , obtained from the student module and the teacher module, respectively.

(ii) $\mathcal{L}_{\mathbf{S}-\text{func}}$ indicates the functional consistency loss. *Motivated by clinical priors, brain regions belonging to the same functional network typically exhibit similar aging rates; large discrepancies within a network are uncommon (see Sec. D).* Based on this prior, for each subject n , we first compute the network-wise mean regional age and then penalize deviations of regions within the same network from

this mean. The loss can be formulated as:

$$\hat{\mu}^{(k,n)} = \frac{1}{|\mathcal{G}^{(k)}|} \sum_{r \in \mathcal{G}^{(k)}} \hat{y}_{\mathbf{S}-\text{final}}^{(r,n)}, \quad (17)$$

$$\mathcal{L}_{\mathbf{S}-\text{func}} = \frac{1}{N} \sum_{n=1}^N \sum_{k=1}^K \frac{1}{|\mathcal{G}^{(k)}|} \sum_{r \in \mathcal{G}^{(k)}} \left| \hat{y}_{\mathbf{S}-\text{final}}^{(r,n)} - \hat{\mu}^{(k,n)} \right|, \quad (18)$$

where $\mathcal{G}^{(k)}$ denotes the k -th brain network, and $\hat{\mu}^{(k,n)}$ denotes, for subject n , the mean predicted age across the regions contained in network k .

4. Metric

As outlined in Challenge-Eval, the lack of region-level ground truth makes conventional evaluation infeasible. We therefore introduce Healthy Control Similarity (HCS) to assess statistical consistency and Neuro-Disease Correlation (NDC) to assess factual consistency, providing an indirect yet testable validation. *Notably, the two metrics are complementary: HCS measures population-level consistency on unseen HCs but is less sensitive to region-wise mode collapsing, whereas NDC probes disease-implicated regions (e.g., PD, AD), confirming the expected elevations versus HCs and exposing regional gradients that HCS may miss.*

4.1. Healthy Control Similarity

The training data consists solely of HC, denoted $\mathcal{D}_{\text{tr}}^{\text{HC}}$. At test stage, we use the unseen HC during training, denoted $\mathcal{D}_{\text{ts}}^{\text{HC}}$ ($\mathcal{D}_{\text{tr}}^{\text{HC}} \cap \mathcal{D}_{\text{ts}}^{\text{HC}} = \emptyset$). For each brain region, we compute the ΔReBA on $\mathcal{D}_{\text{ts}}^{\text{HC}}$ and statistically compare its distribution with the corresponding distribution from $\mathcal{D}_{\text{tr}}^{\text{HC}}$.

Formally, we compute the regional brain age gap as:

$$\Delta\text{ReBA}^{(r,n)} = \hat{y}_{\mathbf{S}-\text{final}}^{(r,n)} - y_{\text{chron}}^{(n)}, \quad (19)$$

where $\Delta\text{ReBA}^{(r,n)}$ is the region r 's brain age gap for subject n . Let $\mathcal{H}_{\text{tr}}^{(r)} = \{\Delta\text{ReBA}^{(r,n)}, n \in \mathcal{D}_{\text{tr}}^{\text{HC}}\}$ and $\mathcal{H}_{\text{ts}}^{(r)} = \{\Delta\text{ReBA}^{(r,n)}, n \in \mathcal{D}_{\text{ts}}^{\text{HC}}\}$ denote the training and test distributions of brain age gaps for region r . Define the per-region HCS via a statistical similarity function as:

$$\text{HCS}^{(r)} = 1 - \Phi_{\text{MMD}} \left(\mathcal{H}_{\text{tr}}^{(r)}, \mathcal{H}_{\text{ts}}^{(r)} \right), \quad (20)$$

where Φ_{MMD} is the function of Maximum Mean Discrepancy (MMD) (see Sec. E for more details). $\text{HCS}^{(r)} \in [0, 1]$. **Higher HCS indicates better distributional alignment and, consequently, more accurate predictions.**

4.2. Neuro Disease Correlation

Guided by clinical knowledge and prior literature (Sarasso et al., 2021; Liu et al., 2020), we predefine disease-associated brain regions (e.g., regions 3,4,7,26 for PD,

please see Sec. D Tab. 4 for more details). Patients with the relevant disorder typically show accelerated atrophy in the corresponding regions, causing the predicted ReBA of the disease-associated brain regions to exceed chronological age. Accordingly, for patients with a confirmed diagnosis, NDC computes the ΔReBA between the corresponding regional brain age and the patient's chronological age according to Eq. (19).

Define the disease of patient as $\mathcal{D}_{\text{ts}}^{\text{Disease}} \in \{\mathcal{D}_{\text{ts}}^{\text{PD}}, \mathcal{D}_{\text{ts}}^{\text{AD}}, \dots\}$, the set of disease-associated brain regions is:

$$\mathcal{R}_{\text{ts}}^{\text{Disease}} = \text{Select}(\mathcal{D}_{\text{ts}}^{\text{Disease}}). \quad (21)$$

The per-subject NDC can be formulated as:

$$\text{NDC}^{(n)} = \frac{1}{|\mathcal{R}_{\text{ts}}^{\text{Disease}}|} \sum_{r \in \mathcal{R}_{\text{ts}}^{\text{Disease}}} \frac{1}{1 + e^{-\Delta\text{ReBA}^{(r,n)}}}. \quad (22)$$

$\text{NDC}^{(n)} \in [0, 1]$. **Higher NDC indicates stronger alignment with disease-characteristic regional patterns and, consequently, more credible ReBA estimates.**

5. Experiments

Data. The data are split into training and test sets (please see Sec. G Tab. 5). The training set contains 6,530 raw T1-weighted MRIs from 17 public datasets, comprising HC only, comprising HC only. The test set has three parts: 1,057 unseen HC from other 9 public datasets and our in-house collection, used for the HCS metric; 326 PD cases from PPMI (Marek et al., 2011) and our in-house collection, used for NDC; and 107 AD cases from ADNI (Mueller et al., 2005), also used for NDC. All data will be public.

Implementation. Our model was trained for 60 epochs using the AdamW optimizer, configured with an initial learning rate of 1×10^{-4} and a weight decay of 1×10^{-5} . The learning rate schedule followed a cosine annealing strategy. Several key hyperparameters were involved in training, including $\alpha = 1$, $\eta = 0.1$, and $\zeta = 1$ (see Sec. G for sensitivity analysis). All experiments were conducted on an NVIDIA RTX vGPU. The training batch size was set to 4. The code will be publicly.

Comparison on HCS Metric. HCS quantifies, for each region, how closely the ΔReBA distributions match between training and test sets; higher similarity indicates better prediction for that region (see Fig. 3). Using the Harvard-Oxford atlas (Jenkinson et al., 2012), we parcellate the brain into 48 regions. Fig. 3 reports similarities for four exemplar regions (see Sec. G for more details) and the average results based on 3D DenseNet backbone (Lee et al., 2022a). The ΔReBA similarity for the same region is consistently high, exceeding 73%, validating the effectiveness of our approach.

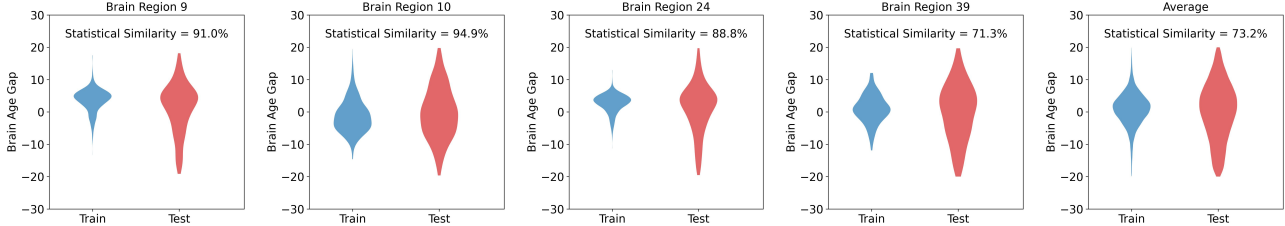


Figure 3. Healthy Control Similarity (HCS) across brain regions (see Sec. G for more regions’ results). Results are based on the 3D DenseNet backbone (Lee et al., 2022a). Blue bars denote the Δ ReBA distributions predicted by our model on training HC; red bars denote the corresponding predictions on test HC. Statistical similarity is computed via Eq. (20). Higher is better. The results show consistently high statistical similarity at the regional level, with an overall HCS reaching 73%, which supports the effectiveness of our method.

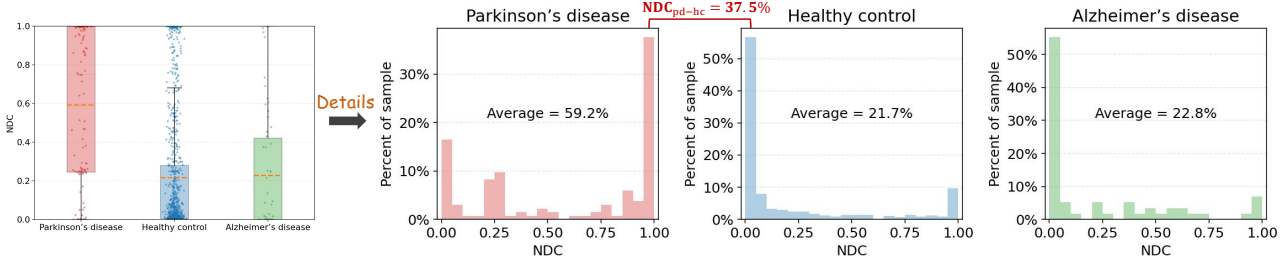


Figure 4. Neuro-Disease Correlation (NDC) for Parkinson’s disease (PD). We focus on regions 3, 4, 7, 26, all of which show clinical evidence of accelerated aging in PD. Accordingly, the Δ ReBA in these regions is expected to exceed those observed in healthy controls (HC) and Alzheimer’s disease (AD). We compute the NDC and compare it across PD, HC, and AD. As anticipated, PD exhibits a markedly higher NDC than both HC and AD, providing indirect support for the accuracy of the proposed ReBA prediction.

Teacher		Student		HCS	NDC _{pd-hc}
Initial ReBA	Soft ReBA	FiLM	$\mathcal{L}_{S\text{-func}}$		
①			✓	✓	17.9 17.5
②	✓		✓	✓	67.5 28.6
③	✓	✓			71.3 6.2
④	✓	✓		✓	72.2 14.3
⑤	✓	✓	✓		61.2 24.8
⑥	✓	✓	✓	✓	73.2 37.5

Table 1. Ablation study (%). HCS and NDC are the proposed metrics. NDC_{pd-hc} is computed on PD-implicated regions as the difference between the NDC of the PD cohort and that of HC.

Comparison on NDC Metric. NDC incorporates clinical priors (see Sec. D) into evaluation: for a given disease, it prespecifies the set of related brain regions and tests whether those regions that “should age earlier” indeed do so. Fig. 4 takes PD as an example (see Sec. G for other diseases); clinically, PD is known to show accelerated aging in regions 3, 4, 7, and 26. Accordingly, we compute the NDC score of these four regions and take the average, and we compare its distribution across the PD, HC, and AD cohorts. The NDC for PD is about 60%, markedly higher than 20% for HC and AD, thereby indirectly confirming the validity of the ReBA estimates.

Ablation Studies. Our method comprises Teacher and Student components. We assess each module via ablation; detailed results appear in Tab. 1. We report HCS and NDC_{pd-hc},

Backbone	Param	Time	HCS	NDC _{pd-hc}
M3T (Jang & Hwang, 2022)	3.9M	568.8min	17.5	21.0
ViT3D (Chen et al., 2023)	1.5M	86.4min	20.6	15.3
Swin3D (Chen et al., 2023)	7.3M	133.2min	18.2	15.1
SwinUNETR (Tang et al., 2022)	52.6M	421.2min	18.3	1.34
AE-FLOW (Zhao et al., 2023)	56.9M	218.4min	48.7	20.4
S3D (Wald et al., 2025)	16.8M	202.8min	65.3	28.6
3D DenseNet (Lee et al., 2022a)	76.5M	94.8min	73.2	37.5

Table 2. Comparison (%) of different backbones. Most results are reported with the 3D DenseNet. M3T, ViT3D, Swin3D, and SwinUNETR are based on the Transformer architecture, AE-FLOW, S3D and 3D DenseNet are based on the CNN architecture.

where is computed on PD-implicated regions as the difference between the NDC of the PD and HC.

For Teacher. (i) Row ① supervises the Student directly with chronological age. Compared with Row ⑥, both HCS and NDC_{pd-hc} drop sharply, indicating that coarse WBA labels cannot be used to predict ReBA and underscoring the necessity of the Teacher. (ii) Row ② adopts the initial ReBA from Eq. (5) as the distillation target. Compared with Row ⑥, HCS and NDC_{pd-hc} decline by about 7-9 %, confirming that the additive regional correction is critical for producing high-quality soft targets for effective Student learning.

For Student. (i) Row ③ removes the Student entirely, leading to 2% drop in HCS and a dramatic 30% drop in NDC_{pd-hc}, underscoring the critical role of the Student. (ii)

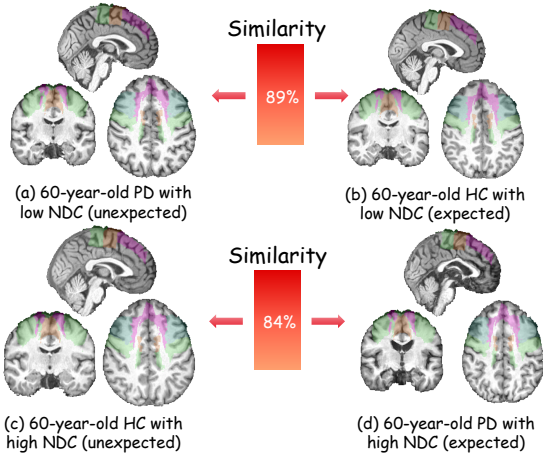


Figure 5. Failure case visualization. (a) and (c) are failures: (a) PD with low NDC resembles the HC in (b); (c) HC with high NDC resembles the PD in (d). Morphometric similarity in PD-related regions likely drives the unexpected NDC.

Row ④ excludes the FiLM block. While HCS remains similar, NDC_{pd-hc} decreases by about 22 %. FiLM introduces region-dependent affine modulation via learnable prompts, enabling individualized readout; without it, regional predictions become homogeneous, which has little effect on HCS but substantially harms NDC. (iii) Row ⑤ omits the functional-consistency loss. HCS and NDC decrease 12–13%, demonstrating that this constraint helps suppress erratic variance while preserving meaningful gradients.

Different Backbones. Our framework is model-agnostic and compatible with standard backbones. Most results are reported with the 3D DenseNet (Lee et al., 2022a) (CNN). We also evaluate alternative CNN backbones, including AE-FLOW (Zhao et al., 2023), S3D (Wald et al., 2025), as well as Transformer-based backbones, including M3T (Jang & Hwang, 2022), ViT3D (Chen et al., 2023), Swin3D (Chen et al., 2023), SwinUNETR (Tang et al., 2022). Comparison results are listed in Tab. 2.

Failure Cases and Analysis. As shown in Fig. 4 (left 2), some PD patients exhibit unexpectedly low NDC values, while in the left 3 and 4, several HC and AD subjects show abnormally high NDC values. These observations deviate from our expectations, so we conducted a focused analysis.

Beyond the intrinsic limitations and uncertainty of the model itself, several factors may contribute to these atypical outcomes: (i) Some participants have inaccurate or unreliable age records, directly affecting NDC. (ii) Early-stage PD patients may show minimal structural change, yielding limited regional brain-age elevation and thus lower NDC. Fig. 5 (a) depicts a 60-year-old PD patient with low NDC (unexpected), whereas Fig. 5 (b) shows an age-matched HC with a similarly low NDC (expected). The two exhibit highly similar morphometric patterns in PD-implicated regions,

which likely explains the PD case’s unexpected outcome. (iii) Some HC or AD subjects may actually be prodromal or high-risk PD individuals, showing accelerated aging in PD-related regions and consequently elevated NDC values. Fig. 5(c) presents a 60-year-old HC with high NDC (unexpected), while Fig. 5(d) shows a 60-year-old PD patient with high NDC (expected). These two share highly similar morphometric patterns in PD-implicated regions, which explains the HC case’s unexpected outcome.

6. Discussion

The aim of this work is to predict ReBA. In the absence of regional clinical ground truth, standard metrics (e.g., MAE) are inapplicable. Instead, we introduce two statistically sound and clinically aligned indirect metrics. This raises a core question: *if the model performs well on these metrics, can it be used in practice?* We believe yes. **The ultimate goal of ReBA is not to recover an absolute “true” regional age, but to reveal regional abnormalities, early risks, or developmental deviations.** Our model identifies condition-specific departures from expected aging patterns, helping clinicians flag regions that merit targeted follow-up and providing researchers with valuable scientific insights. Thus, even without direct ground-truth validation, the approach remains both scientifically and clinically impactful.

7. Conclusion and Future Work

Conclusion. This paper presents the first complete framework for ReBA prediction. To address the lack of fine-grained ground-truth labels, we adopt a Teacher–Student training paradigm in which the Teacher generates soft labels to supervise the Student, yielding stable and interpretable ReBA estimates. For validation, we introduce two complementary metrics (HCS and NDC) that constrain the model from the perspectives of statistical consistency and factual consistency. Experimental results demonstrate the effectiveness of the proposed method.

Limitations and Future Work. (i) Training. We observe residual failure cases failure cases, many of which cannot yet be clearly ascribed to model limitations versus external confounders, hindering wider deployment. Future work will integrate clinical expertise, tighten data quality control, and incorporate uncertainty estimation and cross-site calibration to further improve accuracy. (ii) Validation. Current validation is necessary but not sufficient: NDC depends on clinical priors, and robust priors and data are scarce beyond a few diseases (e.g., PD, AD). To broaden applicability without increasing labeling burden, we plan to develop more accessible validation routes by leveraging longitudinal follow-up and routinely collected clinical scales and imaging biomarkers to derive finer-grained, severity-aware indices as proxy ground truths, thereby keeping validation cost-conscious while enabling more clinically meaningful evaluation.

Appendix

A. Abbreviation

This paper contains numerous abbreviations. For ease of reading, important abbreviations are listed in Tab. 3.

B. Supplemented Related Work

Brain age has emerged as a widely used imaging biomarker that captures the apparent biological aging of an individual’s brain relative to their chronological age. It provides a compact, interpretable indicator with broad utility in population health assessment, early disease screening, risk stratification, and longitudinal monitoring of neurodegeneration. As large neuroimaging cohorts and deep learning continue to evolve, estimating brain age from structural MRI has become a key task in computational neuroscience.

Whole brain age (WBA). Research on WBA is relatively mature. Early work relied on voxel-based morphometry (VBM) features (Ashburner & Friston, 2000; Good et al., 2001; Pennanen et al., 2005), where voxelwise gray- and white-matter measures were summarized into handcrafted descriptors and fed into regression models. Despite their influence, VBM-based methods were constrained by sensitivity to registration quality, smoothing parameters, partial-volume effects, and scanner variability—issues that undermined predictive accuracy and cross-site robustness. Subsequent studies explored classical machine-learning regressors such as Gaussian processes (Cole et al., 2015), hidden Markov models (Wang & Pham, 2011), and random forests (Liem et al., 2017), typically using VBM or global T1-MRI features. With the advent of large datasets and modern compute, deep learning became the dominant paradigm. Recent approaches based on 3D CNNs and Transformer-style architectures directly ingest volumetric MRI and learn age-related patterns end-to-end (Lee et al., 2022a; Cheng et al., 2021; Armanious et al., 2021; Jónsson et al., 2019; Kuchcinski et al., 2023; Yu et al., 2024; Seitz-Holland et al., 2024). While WBA protocols are now standardized, the metric inherently collapses all spatial information into a single scalar. This global averaging dilutes regionally specific signals—crucial for heterogeneous conditions like Parkinson’s or Alzheimer’s disease—masking disease-relevant deviations and limiting interpretability.

Regional brain age (ReBA). In contrast to the mature field of WBA, ReBA estimation remains at a nascent stage. Despite the clear potential of regional granularity, the existing literature, for examples, (Kaufmann et al., 2019; Taylor et al., 2022; Lee et al., 2022b; Busby et al., 2024; Bethlehem et al., 2022), predominantly relies on a *feature-based, two-stage paradigm*. In these frameworks, regional descriptors (e.g., cortical thickness, subcortical volumes) must first

be derived using morphometric packages like FreeSurfer before being fed into downstream statistical models or regressors. While these studies have successfully highlighted that disease-specific aging patterns exist and carry clinical value, their reliance on pre-extracted scalar features introduces a fundamental bottleneck. As noted in the main text, this approach inherently discards rich, high-dimensional spatial information (such as local texture and intensity gradients) and binds the final performance to the success of complex preprocessing pipelines. Even recent extensions, such as the lobar-level predictions by Kalc *et al.* (Bethlehem et al., 2022) or the post-hoc disparity indices by Wu *et al.* (Wu et al., 2025), operate within or atop these feature-constrained limitations. Consequently, the field lacks a general-purpose framework capable of learning regional aging patterns directly from voxel-wise MRI data in an end-to-end manner, a gap our ReBA-Pred-Net is designed to fill.

C. MRI Pre-processing

Due to variations in resolution, contrast, and signal-to-noise ratio across MRI scanners, as well as substantial inter-subject differences in brain size, shape, and anatomical structure, we propose MRI-Processor to standardize all raw T1-weighted MRI scans through a three-step pre-processing pipeline to enhance the robustness of downstream modeling and improve cross-subject comparability: (1) Brain extraction: Remove the skull and non-brain tissues to isolate the brain parenchyma, reducing irrelevant background noise; (2) Bias field correction: Correct intensity inhomogeneities caused by magnetic field non-uniformities, improving overall image intensity uniformity and comparability; and (3) Nonlinear registration: Align each MRI scan to the Montreal Neurological Institute (MNI) standard template to reduce anatomical variability between subjects and facilitate cross-subject analysis and model generalization. This entire workflow was implemented using mature open-source toolkits. We use the DeepPrep (Ren et al., 2025) to complete these steps. The flowchart is shown in Fig. 6.

D. Clinical Prior Knowledge

The human brain can be subdivided into multiple regions according to anatomical and functional characteristics. In this study, we use the Harvard–Oxford Atlas (Jenkinson et al., 2012) for standardized parcellation, ensuring consistent region definitions across all subjects. Regions that share similar functional roles can further be grouped into brain networks, which reflect coordinated activity and shared neurobiological functions. A schematic illustration of these region-to-network mappings is shown in Fig. 7.

Neurodegenerative diseases typically do not affect the brain uniformly. In Parkinson’s disease (PD), pathological

No.	Abbreviation	Full Name
1	WBA	Whole brain age
2	ReBA	Regional brain age
3	Δ ReBA	Regional brain age gap, <i>i.e.</i> , ReBA minus chronological age
4	HCS	Metric of Healthy Control Similarity
5	NDC	Metric of Neuro Disease Correlation
6	HC	Healthy Control
7	PD	Parkinson's disease
8	AD	Alzheimer's disease
9	MRI	Magnetic Resonance Imaging
10	MAE	Metric of Mean absolute error
11	MSE	Metric of Mean squared error
12	SRCC	Metric of Spearman's rank correlation coefficient
13	FiLM	Feature-wise Linear Modulation

Table 3. Abbreviations.

changes are concentrated in regions involved in motor control, executive function, and affective regulation, while other regions remain relatively preserved. Alzheimer's disease (AD), in contrast, exhibits early and prominent degeneration in memory-related and association cortices—such as the medial temporal lobe, posterior cingulate cortex, and parietal association areas—before spreading to broader cortical systems. This spatial heterogeneity has been consistently reported in prior neuropathological and neuroimaging studies (Gao & Wu, 2016; Burciu & Vaillancourt, 2018).

Building on clinical expertise and existing evidence, we categorize each atlas-defined region into one of three relevance levels for PD and AD: strongly-associated, potentially-associated, and non-associated. These assignments, summarized in Tab. 4, serve as disease-informed priors that guide the interpretation of region-specific aging patterns in our analyses.

E. Bias Correction

In brain age prediction, a common artifact is age bias: predicted age shifts with chronological age, typically overestimating younger individuals and underestimating older ones. This induces a strong correlation between the prediction error and age, undermining evaluation. To mitigate this, we perform brain-region-level bias correction by using the training set (composed entirely of healthy controls). The steps can be formulated as:

$$\mathcal{F}_{\text{bias}}(y_{\text{chron}}^{(n)}) = (\lambda_0^{(r)} + \lambda_1^{(r)} y_{\text{chron}}^{(n)}) - y_{\text{chron}}^{(n)}, \quad (23)$$

$$\hat{y}_{\text{correct}}^{(r)} = \hat{y}_{\text{final}}^{(r)} - \mathcal{F}_{\text{bias}}(y_{\text{chron}}^{(n)}), \quad (24)$$

where $\mathcal{F}_{\text{bias}}$ denotes the bias function; $\lambda_0^{(r)}, \lambda_1^{(r)}$ are brain-region-specific regression coefficients fitted on healthy con-

trols; $\hat{y}_{\text{correct}}^{(r)}$ indicates the corrected brain age of the r -th region, which is the final output.

F. Supplemented Details of Metric

In our main text, we use the function of Maximum Mean Discrepancy (MMD). Here, we show the details of MMD.

Define the training and test distributions of brain age gaps for region r as:

$$\mathcal{H}_{\text{tr}}^{(r)} = \{\Delta\text{ReBA}^{(r,n_{\text{tr}})}, n_{\text{tr}} \in \mathcal{D}_{\text{tr}}^{\text{HC}}\}_{n_{\text{tr}}=1}^{N_{\text{tr}}}, \quad (25)$$

$$\mathcal{H}_{\text{ts}}^{(r)} = \{\Delta\text{ReBA}^{(r,n_{\text{ts}})}, n_{\text{ts}} \in \mathcal{D}_{\text{ts}}^{\text{HC}}\}_{n_{\text{ts}}=1}^{N_{\text{ts}}}, \quad (26)$$

Define the Radial Basis Function (RBF) kernel as:

$$k(a, b) = \exp\left(-\frac{(a-b)^2}{2m^2}\right), \quad (27)$$

where m is the median of $\mathcal{H}_{\text{tr}}^{(r)} \cup \mathcal{H}_{\text{ts}}^{(r)}$.

$$\begin{aligned} \Phi_{\text{MMD}} &= \frac{1}{N_{\text{tr}}(N_{\text{tr}-1})} \sum_{n_{\text{tr}} \neq n'_{\text{tr}}} k\left(\Delta\text{ReBA}^{(r,n_{\text{tr}})}, \Delta\text{ReBA}^{(r,n'_{\text{tr}})}\right) \\ &+ \frac{1}{N_{\text{ts}}(N_{\text{ts}-1})} \sum_{n_{\text{ts}} \neq n'_{\text{ts}}} k\left(\Delta\text{ReBA}^{(r,n_{\text{ts}})}, \Delta\text{ReBA}^{(r,n'_{\text{ts}})}\right) \\ &- \frac{2}{N_{\text{tr}}N_{\text{ts}}} \sum_{n_{\text{tr}}, n_{\text{ts}}} k\left(\Delta\text{ReBA}^{(r,n_{\text{tr}})}, \Delta\text{ReBA}^{(r,n_{\text{ts}})}\right) \end{aligned} \quad (28)$$

G. Supplemented Experiments

The details about data are listed in Tab. 5.

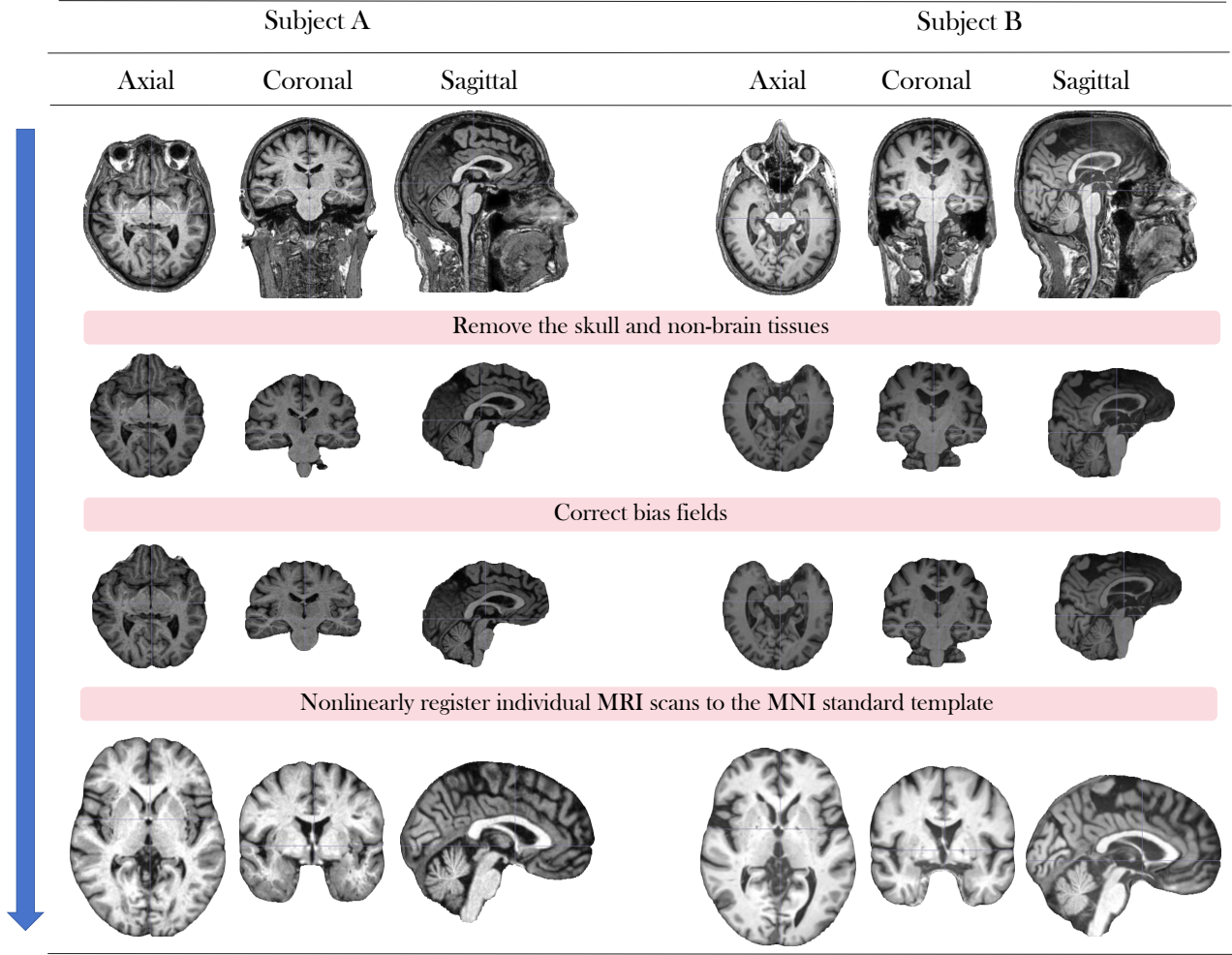


Figure 6. Flowchart of MRI Pre-processing.

G.1. Comparison on HCS Metric

For the HCS metric, the main text reports results for only five representative brain regions. The Harvard–Oxford atlas used in our study, however, contains 48 regions in total. Here, we provide the complete set of HCS values for all regions: Regions 1–25 are shown in Fig. 8, while Regions 26–48 and the overall average are presented in Fig. 9.

G.2. Comparison on NDC Metric

The NDC metric incorporates clinical priors by specifying, for each disease, a set of regions expected to exhibit accelerated aging. It then evaluates whether these regions indeed show higher ReBA in affected individuals. In the main text, we presented results using PD as an example. Here, we report the corresponding analysis for AD in Fig. 10. Clinically, AD is known to involve accelerated degeneration in regions 8–16, 20–23, 30, 31, 34, 35, 37–39. Based on these priors, we compute the NDC score by averaging the

regional brain-age gaps over this set of AD-related regions and compare the resulting distributions across AD, HC, and PD subjects. The NDC for AD reaches approximately 0.71, which is substantially higher than that of HC (0.3) and PD (0.4), providing additional evidence supporting the validity of our regional brain-age estimation

G.3. Training Loss Curve

Our framework consists of two components, Teacher and Student. In Fig. 11, we plot the training losses for both stages. The curves for the teacher and student losses decrease steadily without oscillation, indicating that the optimization is stable and both models converge properly. This suggests that our training strategy for the teacher–student framework is effective and does not suffer from obvious optimization difficulties or collapse.

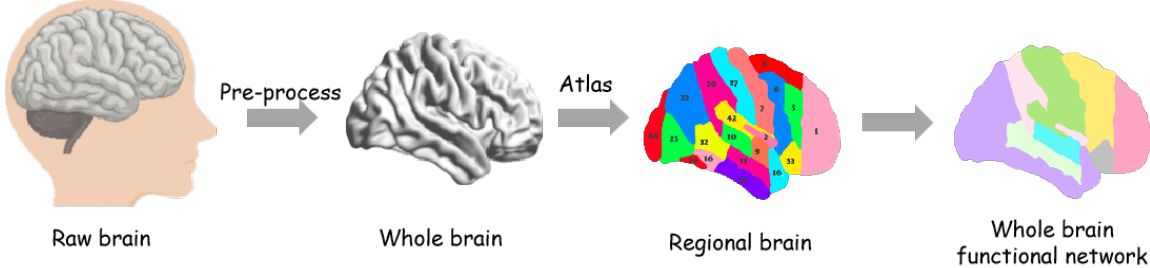


Figure 7. Illustration of the mapping from atlas-defined brain regions to functionally coherent brain networks.

G.4. Sensitivity Analysis of Hyperparameters

In this study, we consider three hyperparameters that noticeably influence model performance. In the main experiments, we set them to $\alpha = 1$, $\eta = 0.1$, and $\zeta = 1$. To examine how each parameter affects the results, we conduct a one-factor analysis where we vary a single parameter while keeping the other two fixed. See Fig. 12.

For NDC (top row), the model is clearly sensitive to all three hyperparameters. Changing α within $[0, 1.5]$ leads to a marked rise and subsequent drop in NDC, and varying η induces an even stronger effect, with NDC decreasing sharply when η exceeds a small range around 0.1. The NDC score also increases and then declines as ζ grows, indicating a relatively narrow high-performing interval. These trends suggest that the choice of α , η , and ζ must be made carefully when optimizing NDC.

For HCS (bottom row), the curves are comparatively flatter. Although there is a mild peak around the default setting ($\alpha = 1$, $\eta = 0.1$, $\zeta = 1$), the fluctuations in HCS across the explored ranges are much smaller than those observed for NDC. This indicates that our method is relatively robust with respect to these hyperparameters when evaluated by HCS, while NDC is more sensitive and thus more dependent on precise hyperparameter tuning.

References

Armanious, K., Abdulatif, S., Shi, W., Salian, S., Küstner, T., Weiskopf, D., Hepp, T., Gatzidis, S., and Yang, B. Age-net: an mri-based iterative framework for brain biological age estimation. *IEEE Transactions on Medical Imaging*, 40(7):1778–1791, 2021.

Ashburner, J. and Friston, K. J. Voxel-based morphometry—the methods. *NeuroImage*, 11(6):805–821, 2000.

Avants, B. B., Tustison, N., Song, G., et al. Advanced normalization tools (ants). *Insight j*, 2(365):1–35, 2009.

Bethlehem, R. A., Seidlitz, J., White, S. R., Vogel, J. W., Anderson, K. M., Adamson, C., Adler, S., Alexopoulos, G. S., Anagnostou, E., Areces-Gonzalez, A., et al. Brain charts for the human lifespan. *Nature*, 604(7906):525–533, 2022.

Burciu, R. G. and Vaillancourt, D. E. Imaging of motor cortex physiology in parkinson’s disease. *Movement Disorders*, 33(11):1688–1699, 2018.

Busby, N., Newman-Norlund, S., Sayers, S., Rorden, C., Newman-Norlund, R., Wilmskoetter, J., Roth, R., Wilson, S., Schwen-Blackett, D., Kristinsson, S., et al. Regional brain aging: premature aging of the domain general system predicts aphasia severity. *Communications Biology*, 7(1):718, 2024.

Chen, Z., Agarwal, D., Aggarwal, K., Safta, W., Balan, M. M., and Brown, K. Masked image modeling advances 3d medical image analysis. In *Proceedings of the IEEE/CVF Winter Conference on Applications of Computer Vision*, pp. 1970–1980, 2023.

Cheng, J., Liu, Z., Guan, H., Wu, Z., Zhu, H., Jiang, J., Wen, W., Tao, D., and Liu, T. Brain age estimation from mri using cascade networks with ranking loss. *IEEE Transactions on Medical Imaging*, 40(12):3400–3412, 2021.

Cole, J. H., Leech, R., Sharp, D. J., and Initiative, A. D. N. Prediction of brain age suggests accelerated atrophy after traumatic brain injury. *Annals of Neurology*, 77(4):571–581, 2015.

Fischl, B. Freesurfer. *NeuroImage*, 62(2):774–781, 2012.

Gao, L.-l. and Wu, T. The study of brain functional connectivity in parkinson’s disease. *Translational Neurodegeneration*, 5(1):18, 2016.

Good, C. D., Johnsrude, I. S., Ashburner, J., Henson, R. N., Friston, K. J., and Frackowiak, R. S. A voxel-based morphometric study of ageing in 465 normal adult human brains. *NeuroImage*, 14(1):21–36, 2001.

Jang, J. and Hwang, D. M3t: three-dimensional medical image classifier using multi-plane and multi-slice transformer. In *Proceedings of the IEEE/CVF Computer Vision*

and Pattern Recognition Conference, pp. 20718–20729, 2022.

Jenkinson, M., Beckmann, C. F., Behrens, T. E., Woolrich, M. W., and Smith, S. M. Fsl. *Neuroimage*, 62(2):782–790, 2012.

Jónsson, B. A., Björnsdóttir, G., Thorgerísson, T. E., Ellingsen, L. M., Walters, G. B., Gudbjartsson, D. F., Stefansson, H., Stefansson, K., and Ulfarsson, M. O. Brain age prediction using deep learning uncovers associated sequence variants. *Nature communications*, 10(1):5409, 2019.

Kalc, P., Dahnke, R., Hoffstaedter, F., Gaser, C., and Initiative, A. D. N. Brainage: Revisited and reframed machine learning workflow. *Human Brain Mapping*, 2024.

Kaufmann, T., van der Meer, D., Doan, N. T., Schwarz, E., Lund, M. J., Agartz, I., Alnæs, D., Barch, D. M., Baur-Streubel, R., Bertolino, A., et al. Common brain disorders are associated with heritable patterns of apparent aging of the brain. *Nature Neuroscience*, 22(10):1617–1623, 2019.

Kuchcinski, G., Rumetshofer, T., Zervides, K. A., Lopes, R., Gautherot, M., Pruvost, J.-P., Bengtsson, A. A., Hansson, O., Jönsen, A., and Sundgren, P. C. M. Mri brainage demonstrates increased brain aging in systemic lupus erythematosus patients. *Frontiers in Aging Neuroscience*, 15:1274061, 2023.

Lee, J., Burkett, B. J., Min, H.-K., Senjem, M. L., Lundt, E. S., Botha, H., Graff-Radford, J., Barnard, L. R., Gunter, J. L., Schwarz, C. G., et al. Deep learning-based brain age prediction in normal aging and dementia. *Nature Aging*, 2(5):412–424, 2022a.

Lee, P.-L., Kuo, C.-Y., Wang, P.-N., Chen, L.-K., Lin, C.-P., Chou, K.-H., and Chung, C.-P. Regional rather than global brain age mediates cognitive function in cerebral small vessel disease. *Brain Communications*, 4(5):fcac233, 2022b.

Liem, F., Varoquaux, G., Kynast, J., Beyer, F., Masouleh, S. K., Huntenburg, J. M., Lampe, L., Rahim, M., Abraham, A., Craddock, R. C., et al. Predicting brain-age from multimodal imaging data captures cognitive impairment. *NeuroImage*, 148:179–188, 2017.

Liu, C., Jiang, J., Zhou, H., Zhang, H., Wang, M., Jiang, J., Wu, P., Ge, J., Wang, J., Ma, Y., et al. Brain functional and structural signatures in parkinson’s disease. *Frontiers in Aging Neuroscience*, 12:125, 2020.

Marek, K., Jennings, D., Lasch, S., Siderowf, A., Tanner, C., Simuni, T., Coffey, C., Kieburtz, K., Flagg, E., Chowdhury, S., et al. The parkinson progression marker initiative (ppmi). *Progress in Neurobiology*, 95(4):629–635, 2011.

Mueller, S. G., Weiner, M. W., Thal, L. J., Petersen, R. C., Jack, C., Jagust, W., Trojanowski, J. Q., Toga, A. W., and Beckett, L. The alzheimer’s disease neuroimaging initiative. *Neuroimaging Clinics*, 15(4):869–877, 2005.

Pennanen, C., Testa, C., Laakso, M., Hallikainen, M., Hellkala, E., Hänninen, T., Kivipelto, M., Könönen, M., Nissinen, A., Tervo, S., et al. A voxel based morphometry study on mild cognitive impairment. *Journal of Neurology, Neurosurgery & Psychiatry*, 76(1):11–14, 2005.

Ren, J., An, N., Lin, C., Zhang, Y., Sun, Z., Zhang, W., Li, S., Guo, N., Cui, W., Hu, Q., et al. Deepprep: an accelerated, scalable and robust pipeline for neuroimaging preprocessing empowered by deep learning. *Nature Methods*, pp. 1–4, 2025.

Riccardi, N., Teghipco, A., Newman-Norlund, S., Newman-Norlund, R., Rangus, I., Rorden, C., Fridriksson, J., and Bonilha, L. Distinct brain age gradients across the adult lifespan reflect diverse neurobiological hierarchies. *Communications Biology*, 8(1):802, 2025.

Sarasso, E., Agosta, F., Piramide, N., and Filippi, M. Progression of grey and white matter brain damage in parkinson’s disease: a critical review of structural mri literature. *Journal of Neurology*, 268(9):3144–3179, 2021.

Seitz-Holland, J., Haas, S. S., Penzel, N., Reichenberg, A., and Pasternak, O. Brainage, brain health, and mental disorders: A systematic review. *Neuroscience & Biobehavioral Reviews*, 159:105581, 2024.

Tang, Y., Yang, D., Li, W., Roth, H. R., Landman, B., Xu, D., Nath, V., and Hatamizadeh, A. Self-supervised pre-training of swin transformers for 3d medical image analysis. In *Proceedings of the IEEE/CVF Computer Vision and Pattern Recognition Conference*, pp. 20730–20740, 2022.

Taylor, A., Zhang, F., Niu, X., Heywood, A., Stocks, J., Feng, G., Popuri, K., Beg, M. F., Wang, L., Initiative, A. D. N., et al. Investigating the temporal pattern of neuroimaging-based brain age estimation as a biomarker for alzheimer’s disease related neurodegeneration. *NeuroImage*, 263:119621, 2022.

Wald, T., Ulrich, C., Lukyanenko, S., Goncharov, A., Paderno, A., Miller, M., Maerkisch, L., Jaeger, P., and Maier-Hein, K. Revisiting mae pre-training for 3d medical image segmentation. In *Proceedings of the IEEE/CVF Computer Vision and Pattern Recognition Conference*, pp. 5186–5196, 2025.

Wang, B. and Pham, T. D. Mri-based age prediction using hidden markov models. *Journal of Neuroscience Methods*, 199(1):140–145, 2011.

Wang, K., Liu, F., Wu, W., Hu, C., Shen, X., Wang, M., Li, G., Zeng, F., Liu, L., Wong, I. N., et al. A full life cycle biological clock based on routine clinical data and its impact in health and diseases. *Nature Medicine*, pp. 1–11, 2025.

Wu, Y., Sun, S., Zhang, C., Ma, X., Zhu, X., Li, Y., Lin, L., and Fu, Z. Regional brain aging disparity index: Region-specific brain aging state index for neurodegenerative diseases and chronic disease specificity. *Bioengineering*, 12(6):607, 2025.

Yu, Y., Cui, H.-Q., Haas, S. S., New, F., Sanford, N., Yu, K., Zhan, D., Yang, G., Gao, J.-H., Wei, D., et al. Brain-age prediction: Systematic evaluation of site effects, and sample age range and size. *Human Brain Mapping*, 45 (10):e26768, 2024.

Zhao, Y., Ding, Q., and Zhang, X. Ae-flow: Autoencoders with normalizing flows for medical images anomaly detection. In *The Eleventh International Conference on Learning Representations*, 2023.

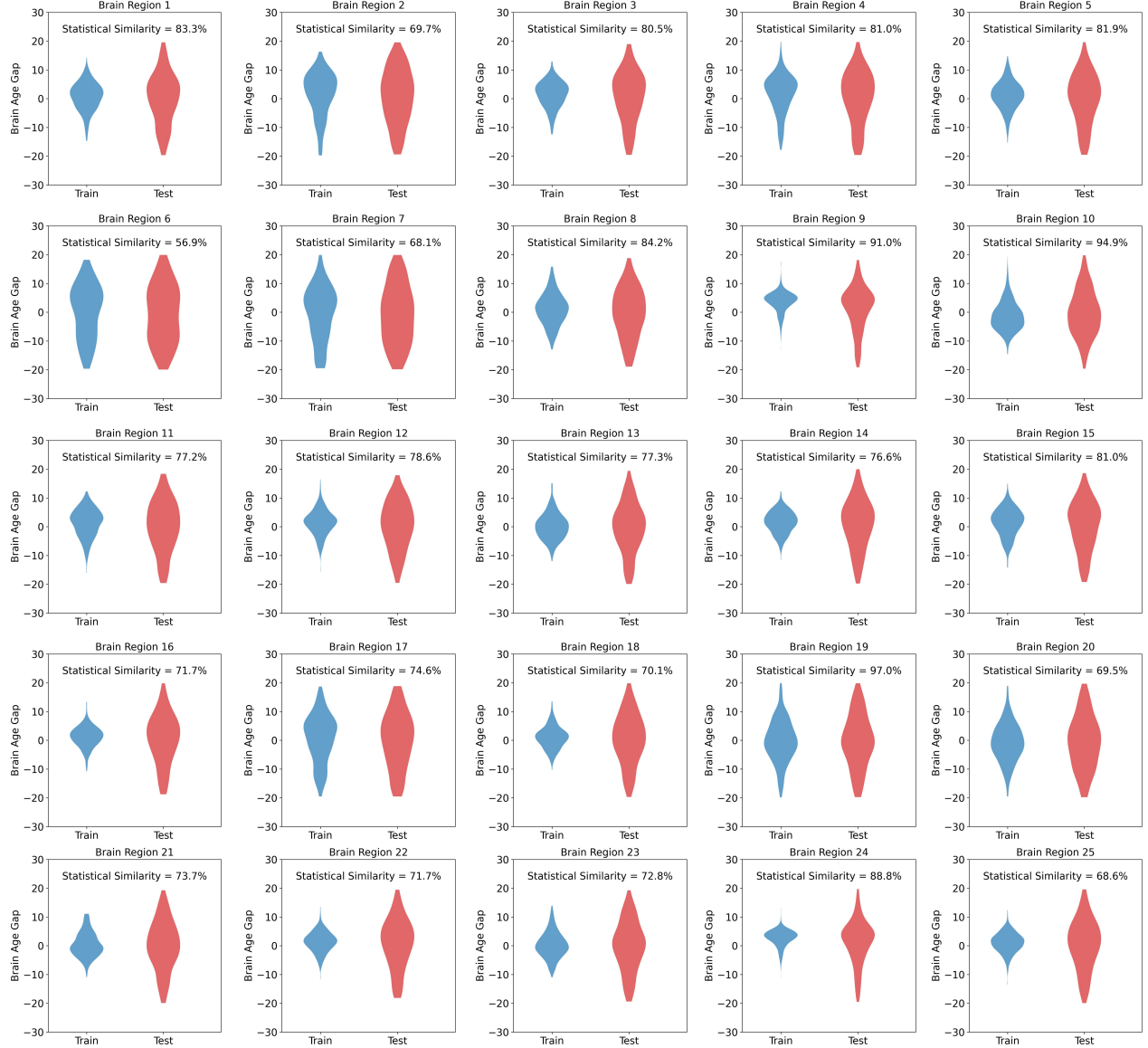


Figure 8. Healthy Control Similarity (HCS) across brain regions (1-25 regions). Results are based on the 3D DenseNet backbone (Lee et al., 2022a). Blue bars denote the Δ ReBA distributions predicted by our model on training HC; red bars denote the corresponding predictions on test HC. Statistical similarity is computed via Main. Eq. (20). Higher is better.

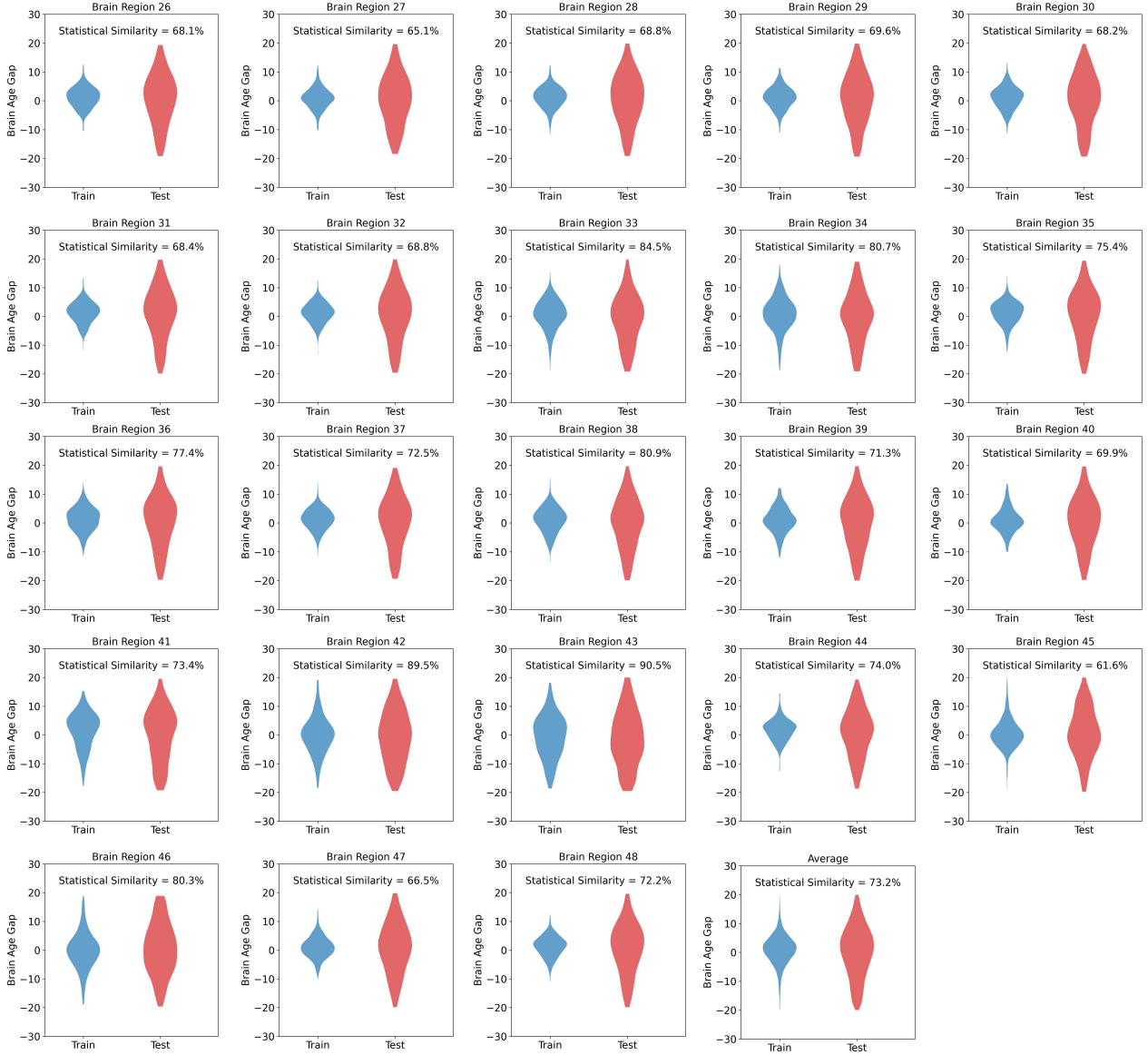


Figure 9. Healthy Control Similarity (HCS) across brain regions (26–48 regions and average). Results are based on the 3D DenseNet backbone (Lee et al., 2022a). Blue bars denote the Δ ReBA distributions predicted by our model on training HC; red bars denote the corresponding predictions on test HC. Statistical similarity is computed via Main. Eq. (20). Higher is better.

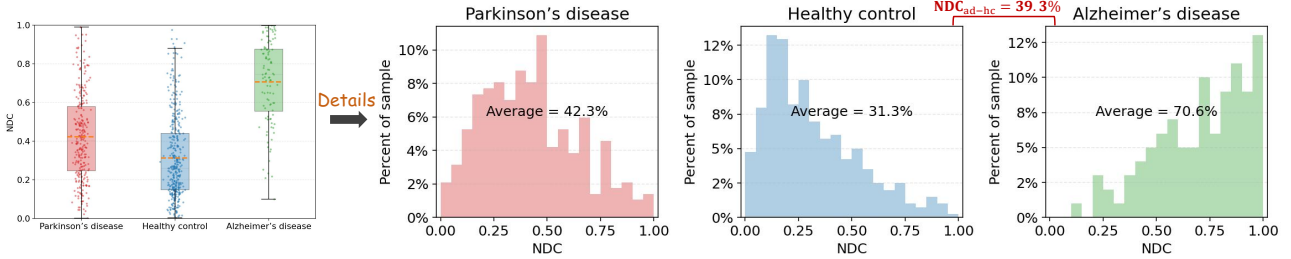


Figure 10. Neuro-Disease Correlation (NDC) for Alzheimer's disease (AD). We focus on regions 8–16, 20–23, 30, 31, 34, 35, 37–39, all of which show clinical evidence of accelerated aging in AD. Accordingly, the Δ ReBA in these regions is expected to exceed those observed in healthy controls (HC) and Parkinson's disease (PD). We compute the NDC and compare it across AD, HC, and PD. As anticipated, AD exhibits a markedly higher NDC than both HC and PD, providing indirect support for the accuracy of the proposed ReBA prediction.

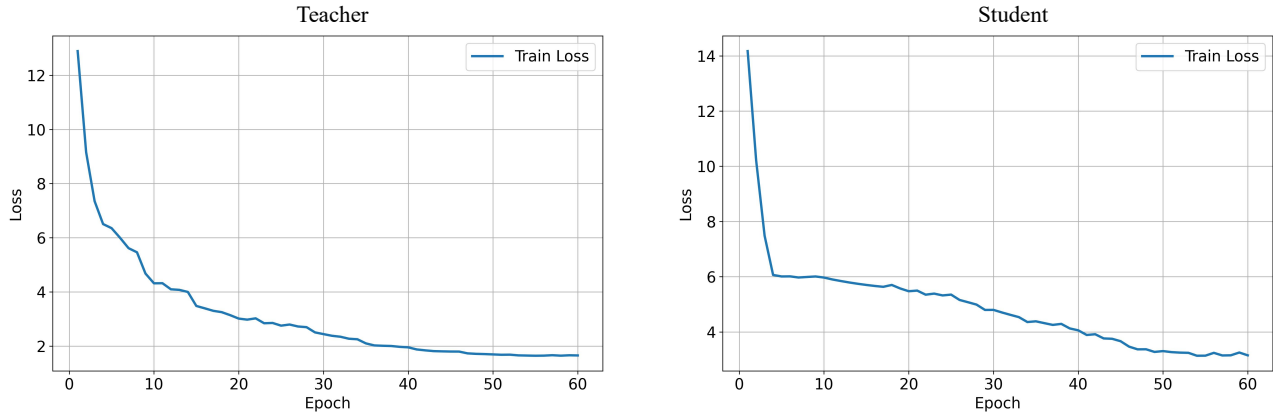


Figure 11. Training loss of Teacher and Student modules.

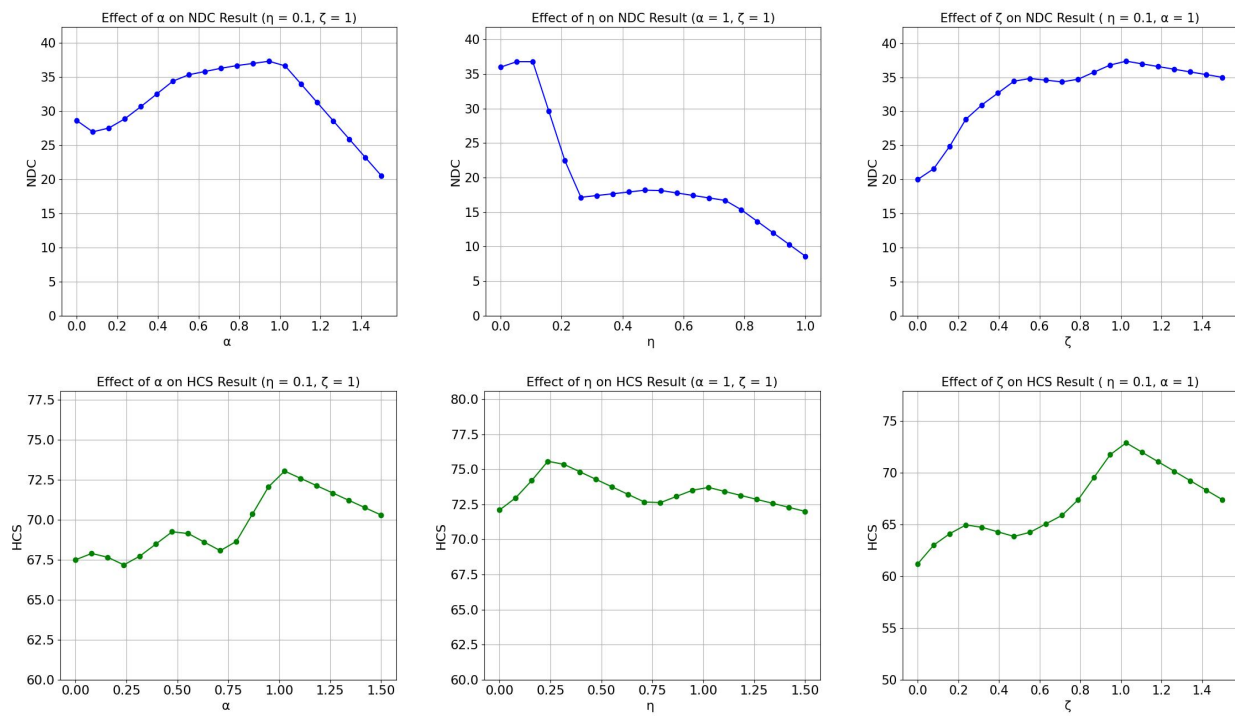


Figure 12. Sensitivity of hyperparameters.

Brain Region No.	Brain Region Name	Relevance with PD	Relevance with AD
1	Frontal Pole	None	Potentially
2	Insular Cortex	Potentially	None
3	Superior Frontal Gyrus	Strong	Potentially
4	Middle Frontal Gyrus	Strong	Potentially
5	Inferior Frontal Gyrus, Triangular Part	Potentially	Potentially
6	Inferior Frontal Gyrus, Opercular Part	Potentially	Potentially
7	Precentral Gyrus	Strong	None
8	Temporal Pole	None	Strong
9	Superior Temporal Gyrus, Anterior Division	None	Strong
10	Superior Temporal Gyrus, Posterior Division	None	Strong
11	Middle Temporal Gyrus, Anterior Division	None	Strong
12	Middle Temporal Gyrus, Posterior Division	None	Strong
13	Temporooccipital Middle Temporal Gyrus	None	Strong
14	Inferior Temporal Gyrus, Anterior Division	None	Strong
15	Inferior Temporal Gyrus, Posterior Division	None	Strong
16	Temporooccipital Inferior Temporal Gyrus	None	Strong
17	Postcentral Gyrus	Potentially	None
18	Superior Parietal Lobule	Potentially	None
19	Supramarginal Gyrus, Anterior Division	None	None
20	Supramarginal Gyrus, Posterior Division	None	Strong
21	Angular Gyrus	Potentially	Strong
22	Lateral Occipital Cortex, Superior Division	None	Strong
23	Lateral Occipital Cortex, Inferior Division	None	Strong
24	Intracalcarine Cortex	None	None
25	Medial Frontal Cortex	Potentially	Potentially
26	Juxtapositional Lobule Cortex (SMA)	Strong	None
27	Subcallosal Cortex	None	None
28	Paracingulate Gyrus	None	None
29	Anterior Cingulate Gyrus	None	None
30	Posterior Cingulate Gyrus	Potentially	Strong
31	Precuneous Cortex	Potentially	Strong
32	Cuneal Cortex	None	Potentially
33	Orbitofrontal Cortex	None	Potentially
34	Parahippocampal Gyrus, Anterior Division	None	Strong
35	Parahippocampal Gyrus, Posterior Division	None	Strong
36	Lingual Gyrus	None	Potentially
37	Temporal Fusiform Cortex, Anterior Division	None	Strong
38	Temporal Fusiform Cortex, Posterior Division	None	Strong
39	Temporooccipital Fusiform Cortex	None	Strong
40	Occipital Fusiform Gyrus	None	Potentially
41	Frontal Operculum Cortex	None	None
42	Central Opercular Cortex	None	None
43	Parietal Operculum Cortex	None	None
44	Planum Polare	None	None
45	Heschl's Gyrus	None	None
46	Planum Temporale	None	None
47	Supracalcarine Cortex	None	None
48	Occipital Pole	None	None

Table 4. Brain regions and their relevance with PD and AD. The 48 cortical regions were categorized into three groups: Strong, Potentially and None. The 48 cortical regions were categorized into three groups: Strong, Potentially, and None. For PD, Strong denotes regions directly involved in motor control; Potentially denotes regions that show significant differences between PD patients and healthy controls and are likely involved in motor modulation; and None denotes regions with weak or insufficient evidence of association with PD. For AD, Strong denotes regions known to undergo early and prominent neurodegeneration; Potentially denotes regions that frequently exhibit structural or functional alterations in AD but with less consistent or secondary involvement; and None denotes regions with limited or currently insufficient evidence supporting a direct association with AD-related pathology.

Group	Dataset Name	Samples	Access URL
HC	AHDC	120	https://openneuro.org/datasets/ds005901
	AgeRisk	187	https://openneuro.org/datasets/ds004711
	AOMIC	928	https://openneuro.org/datasets/ds003097
	AOMIC-PIOP1	226	https://openneuro.org/datasets/ds002790
	AOMIC-PIOP2	216	https://openneuro.org/datasets/ds002785
	BOLD-Variability	158	https://openneuro.org/datasets/ds005270
	Chronotype-Sleep	136	https://openneuro.org/datasets/ds003826
	DLBS	315	https://fcon_1000.projects.nitrc.org/indi/retro/
	DP-pCASL	186	https://openneuro.org/datasets/ds005529
	HCP	35	https://ida.loni.usc.edu/login.jsp
	HRV-Emotion	177	https://openneuro.org/datasets/ds003823
	IXI	581	https://brain-development.org/ixi-dataset/
	LA5c	272	https://openneuro.org/datasets/ds000030
	MR-ART	148	https://openneuro.org/datasets/ds004173
AD	Narratives	345	https://openneuro.org/datasets/ds002345
	NEBULA101	101	https://openneuro.org/datasets/ds005613
	ThinkAloud	118	https://openneuro.org/datasets/ds006067
	TOF-MRA	284	https://openneuro.org/datasets/ds003949
	NKI	974	http://fcon_1000.projects.nitrc.org/indi/enhanced/
	SALD	494	http://fcon_1000.projects.nitrc.org/indi/retro/sald.html
	SLIM	580	http://fcon_1000.projects.nitrc.org/indi/retro/southwestuni_qiu_index.html
	GSP	1006	https://www.neuroinfo.org/gsp
	HC Total	7587	
PD	PPMI	169	https://www.ppmi-info.org/
	In-house collection	157	-
	PD Total	326	
AD	ADNI	107	https://adni.loni.usc.edu/data-samples/adni-data/
	AD Total	107	

Table 5. Summary of Datasets by Group